Available online at www.sciencedirect.com

SciVerse ScienceDirect

Scripta Materialia 67 (2012) 61–64

Scripta MATERIALIA

www.elsevier.com/locate/scriptamat

Structural defects and non-ferroelectric piezoelectricity in an unpoled $SrTiO_3$–$Bi_{12}TiO_{20}$ (ST–BT) composite ceramics

L.J. Zhang,[a] T. Wang,[b] L.H. Wang,[c] J.D. Liu,[a] M.L. Zhao[c] and B.J. Ye[a,*]

[a]*Department of Modern Physics, University of Science and Technology of China, Hefei 230026, People's Republic of China*
[b]*Institute of Fluid Physics, CAEP, P.O. Box 919-106, Mianyang 621900, People's Republic of China*
[c]*School of Physics, Shandong University, Jinan 250100, People's Republic of China*

Received 18 January 2012; revised 2 March 2012; accepted 20 March 2012
Available online 25 March 2012

Anomalous piezoelectricity $SrTiO_3$–$Bi_{12}TiO_{20}$ (ST–BT) composite ceramics fabricated by traditional sintering technology were first studied by positron annihilation lifetime spectroscopy and Doppler broadening spectroscopy. A large number of crystal defects were observed in ST–BT composite ceramics with the sintering temperature below 980 °C. The piezoelectric effect appeared concurrently with a high concentration of single-vacancy defects in the ceramics, suggesting that it may be closely related to the microstructure. This further proves that the flexoelectric effect is the origin of non-ferroelectric piezoelectricity.

Keywords: Ceramics; Piezoelectricity; Positron annihilation; Crystal defects; Flexoelectric effect

Non-ferroelectric piezoelectric materials are promising for high-temperature applications due to their lack of a Curie temperature. These non-ferroelectric piezoelectric materials, including Langasite single crystals, oriented AlN films and polar glass ceramics, have been studied in detail in recent decades [1–5], but they are extremely expensive for their complex production processes. Recently, the traditional sintering technology for non-ferroelectric piezoelectric ceramics has been improved a lot. Zhao et al. [6,7] reported unusual piezoelectricity in $Na_{0.5}Bi_{0.5}TiO_3$-based and $(Na_{0.5}Bi_{0.5})_{0.94}$-$Ba_{0.06}TiO_3$–$Bi_{12}TiO_{20}$ composite ceramics that had been produced by the ordinary sintering technique. A piezoelectric $CaCu_3Ti_4O_{12}$ ceramic material was also reported by Tararam et al. [8]. Now a new type of naturally polarized non-ferroelectric piezoelectric $SrTiO_3$–$Bi_{12}TiO_{20}$ (ST–BT) composite ceramic has been prepared by the conventional solid-state reaction route at Shandong University. This material shows great potential for high-temperature piezoelectric applications.

The actual mechanism of piezoelectricity in non-ferroelectric ceramics that are fabricated by traditional sintering technology is not yet clear. However, the flexoelectric effect is widely accepted as explaining the origin of piezoelectricity [6–12]. The flexoelectric effect, which occurs in the insulating oxides, is the coupling between the mechanical strain gradient and electric polarization induced by inhomogeneous strain in the materials. A strain gradient can be formed in a crystalline structure by lattice mismatch [13–15], impurities [16] or chemical fluctuation in cationic segregation [17]. All of these factors lead to a great number of crystal defects (vacancies, divacancies, interstitials, etc.). In contrast to ferroelectric polarization, which occurs in the whole crystalline structure of non-centrosymmetric crystals, non-ferroelectric piezoelectricity is localized in the volumes with broken symmetry that are subjected to inhomogeneous deformation [8]. If the theory that the flexoelectric effect causes non-ferroelectric piezoelectricity is correct, a high concentration of crystal defects should be found in non-ferroelectric piezoelectric ceramics. Positron annihilation spectroscopy (PAS) is well suited to the nondestructive study of structural defects in solid materials because of its sensitivity to and selectivity of crystal defects [18,19]. Many significant results have already been achieved by applying positron annihilation techniques to ceramic defect studies [20,21]. In this letter, the structural defects and piezoelectricity in non-ferroelectric ST–BT composite ceramics are studied.

* Corresponding author. E-mail: bjye@ustc.edu.cn

1359-6462/$ - see front matter © 2012 Published by Elsevier Ltd. on behalf of Acta Materialia Inc.
http://dx.doi.org/10.1016/j.scriptamat.2012.03.022

We explore the correctness of attributing non-ferroelectric piezoelectricity to the flexoelectric effect.

ST–BT composite ceramics were prepared by the conventional solid-state reaction route. All the starting chemicals, Bi_2O_3, TiO_2 and $SrCO_3$, were of analytical grade, and were mixed at the correct molar ratios to achieve ST–BT stoichiometry. These oxides were ball-milled in alcohol for 14 h, dried, pressed into disks and calcined at 800 °C for 3 h. The disks were then ground and wet-milled again under the same conditions. Subsequently, the dried powders were pressed into 15 mm diameter disks and sintered for 3 h in air at 860, 900, 940 or 980 °C (S1, S2, S3 and S4), respectively. We employed two different PAS techniques to detect the structural defects in the ST–BT composite ceramics. The piezoelectric properties were measured by an Agilent 4294A impedance analyzer and a YE2730A d_{33} meter.

Figure 1 shows the X-ray diffraction (XRD) patterns of the ST–BT composite ceramics prepared at the four different sintering temperatures. The structural analysis mainly indicates that the composite ceramics have a perovskite $SrTiO_3$ phase and a sillenite $Bi_{12}TiO_{20}$ phase. Compared with the XRD peaks of those samples, the intensities of $SrTiO_3$ phase peaks are steady; however, the intensities of $Bi_{12}TiO_{20}$ phase peaks change significantly. In addition, a new Bi_2O_3 phase appears and the $Bi_{12}TiO_{20}$ phase weakens when the sintering temperature rises to 980 °C. That is because the $Bi_{12}TiO_{20}$ is decomposed at high temperature.

The PAS experiments were performed at room temperature. Two PAS techniques were employed to characterize crystal defects in the ST–BT composite ceramics, using radioactive ^{22}Na isotopes as a positron source. First, we undertook a positron lifetime spectrum experiment, the experimental details of which can be found elsewhere [18,19]. The positron lifetime spectra were measured using a fast–fast coincidence system, with a resolution of 220 ps. A 10 μCi ^{22}Na positron source was sandwiched between two identical samples. The total number of counts per spectrum was two million. Each spectrum was fitted using the LIFETIME9 [22] program run with the three-component fitting procedure. The longest lifetime τ_3 and its intensity I_3 were around 2 ns and below 0.5% respectively, without significant variation for all compositions. This component is attributed to the ortho-positronium (o-Ps) annihilation in the source or at the surfaces among the grains in the ceramics, and is ignored in the following discussion. The results of positron lifetime are presented in Table 1. τ_1 is attributed to the lifetime component of the host, which mainly reflects the structural properties of the materials. In the S4 sample, the τ_1 is higher than in the other samples. That indicates a significant change in structure, as confirmed by XRD observations. τ_2 is the defect state lifetime, which is a sensitive parameter related to the various structural defects in materials. I_1 and I_2 are related to intensity and reflect the concentration of the component, respectively. The average lifetime $\tau_{av} = (\tau_1 I_1 + \tau_2 I_2)/(I_1 + I_2)$ could reflect the material's microstructure. The value of τ_{av} remains almost constantly at 232 ps at a sintering temperature below 980 °C, but this value increases sharply to 245 ps in S4. According to the two-state trapping model, the bulk lifetime τ_b can be written as follows: $1/\tau_b = I_1/\tau_1 + I_2/\tau_2$. The ratio τ_2/τ_b can be used to identify the defect types (Table 2) [23].

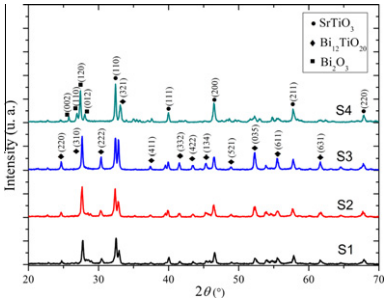

Figure 1. XRD patterns of four ST–BT composite ceramics (S1, S2, S3 and S4). (For interpretation of the references to colour in this figure legend, the reader is referred to the web version of this article.)

Figure 2 shows the lifetime component τ_2 and its intensity I_2. Single-vacancy defects dominate in the S1, S2 and S3 samples, because the values of τ_2/τ_b are around 1.1 in those samples. The I_2 is above 80% and the corresponding concentration of single-vacancy defects is very high. This shows that these samples have serious lattice mismatch and massive crystal defects. τ_2 is larger in the S4 sample than in the others, while the intensity falls significantly. This is because vacancy defects agglomerated and large clusters or microvoids were formed, and the interface states and micropore size increased with the generation of an impurity phase.

In order to obtain more information about which defects are associated with τ_2, coincident Doppler broadening spectroscopy measurements were undertaken (see Fig. 3). Each spectrum collected comprised a total count of over ten million. Figure 3a shows the ratio curves of the coincident Doppler broadening spectra of samples of S1–S4, obtained by normalizing these spectra to the spectrum of Si. The ratio curve of the Si is given as a horizontal line. The shapes of these ratio curves are similar, demonstrating that the chemical environment surrounding the structural free volumes are similar. The peak width (about $P_L = 10 \times 10^{-3} m_0 c$) is large, due to the superposition of positron annihilation with core electrons of different atoms.

Bringing in linear parameters, Doppler broadening is characterized by the *S*-parameter, which reflects the annihilation of positron–electron pairs with a low-momentum distribution (Fig. 3b). Compared to the lifetime spectra, the *S*-parameter reflects the comprehensive effect of various defects. In the samples of S1–S3, the long lifetime τ_2 and its intensity I_2 show no change (Fig. 2), while the *S*-parameter changes significantly. This indicates that the samples have a variety of single-vacancy defects. As the sintering temperature changes, the concentration of each vacancy defect changes inconsistently, but the overall performances are similar to the average lifetime. The *S*–*W* map also illustrates this point because the data cannot fall on a similar linear variation (Fig. 3c).

Figure 4a shows the piezoelectric resonance signals of the ST–BT ceramics at room temperature. The thickness direction of this plate is along the *Z*-axis and the

Table 1. Parameters of positron lifetime spectroscopy of ST–BT composite ceramics with different sintering temperatures.

Sample	τ_1 (ps)	I_1 (%)	τ_2 (ps)	I_2 (%)	τ_{av} (ps)	τ_b (ps)	τ_2/τ_b
S1 (860 °C)	147	11.7	243.6	88.3	232.2978	226.2079	1.076886
S2 (900 °C)	139	7.1	240.1	92.9	232.9219	228.3099	1.051641
S3 (940 °C)	152	19.1	251	80.9	232.091	223.2299	1.124401
S4 (980 °C)	223.7	90.5	453	9.5	245.4835	235.0005	1.927655

Table 2. Criteria of the defect types [23].

	Single-vacancy	Divacancy or trivacancy	Cluster or micro-void
τ_2/τ_b	1–1.2	1.3–1.4	>1.5

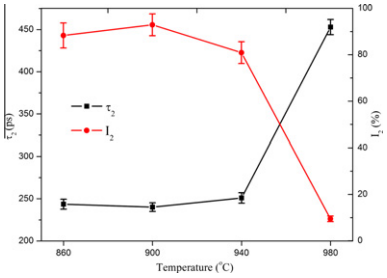

Figure 2. Relationship of positron lifetime τ_2 and I_2 to a series of ST–BT composite ceramics (S1, S2, S3 and S4). Errors are given within error bars, and the values of χ^2 were in the range of 1.0–1.2. (For interpretation of the references to colour in this figure legend, the reader is referred to the web version of this article.)

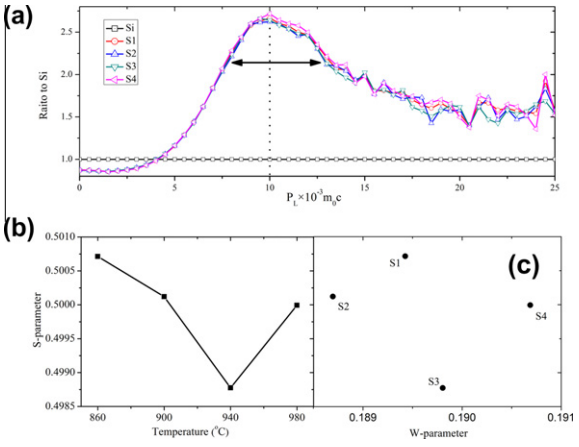

Figure 3. Results of coincident Doppler broadening spectra measured on the four ST–BT composite ceramics (S1, S2, S3 and S4). (a) Ratio curves of the coincidently measured Doppler broadening spectra of a series of ST–BT composite ceramics to Si. (b) Normalized low-momentum annihilation fraction *S*-parameter for the four ST–BT composite ceramics. (c) The interdependence of parameters *S* and *W*. (For interpretation of the references to colour in this figure legend, the reader is referred to the web version of this article.)

electrode face is perpendicular to it. Thickness extension and thickness shear modes were simultaneously observed in S1–S3. Thus, the piezoelectric coefficient d_{33} is not zero, as measured by a YE2730A d_{33} meter (Fig. 4b). Piezoelectric resonance signals could not be measured in S4, indicating that the piezoelectric effect

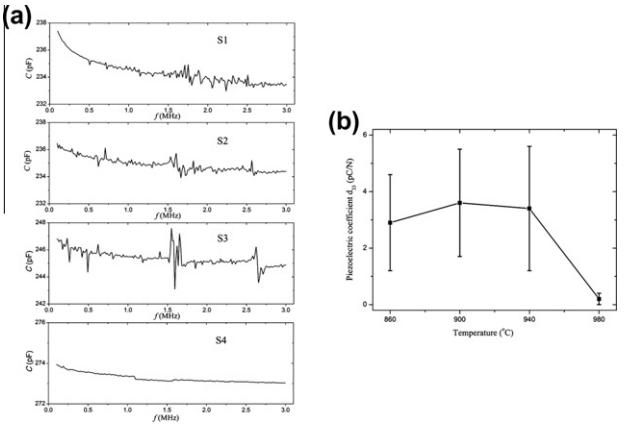

Figure 4. The piezoelectric properties for ST–BT composite ceramics. (a) Piezoelectric resonance signals of ST–BT composite ceramics at different sintering temperatures. (b) Piezoelectric coefficient d_{33} of S1–S4.

disappears when the sintering temperature is raised to 980 °C. Figure 4b also shows the similar piezoelectricity in the three ST–BT composite ceramics S1–S3. Their piezoelectric strain coefficients d_{33} do not remain constant over the entire surface due to the inhomogeneity of the internal structure. Error bars are generated based on data obtained from 50 different locations on each sample. The maximum value of d_{33} is near 6 pC/N. Comparing Figures 2 and 4b, a certain similarity is seen. The lifetime τ_2 of the samples corresponds well with the piezoelectric coefficient d_{33}. The change curve of the lifetime τ_2 corresponds well with the curve of the piezoelectric coefficient d_{33}. From our analysis, ST–BT composite ceramics with a high concentration of single-vacancy defects contain a massive lattice mismatch, which corresponds to a strong piezoelectric property.

In summary, ST–BT composite ceramics were fabricated by a conventional solid-state reaction route. Anomalous piezoelectricity was found in unpoled samples. The piezoelectric effect appeared concurrently with a high concentration of single-vacancy defects in the ceramics, suggesting that it may be closely related to the microstructure. According to the flexoelectric effect, the concentration of crystal defects reflects the degree of lattice mismatch. A serious lattice mismatch could enhance the flexoelectric effect, causing an increase in piezoelectricity. Our results confirm that non-ferroelectric ST–BT composite ceramics with piezoelectricity have massive single-vacancy defects, causing serious lattice mismatch. This provides convincing evidence that the flexoelectric effect is responsible for non-ferroelectric piezoelectricity.

Further experiments are required to explore the whole sintering process and structural defects. Regardless, this new class of ceramics represents a new avenue for research on non-ferroelectric piezoelectric ceramics that are fabricated by traditional sintering technology for high-temperature applications.

This work is supported by the State Key Program of National Science Foundation of China (Grant No. 10835006) and the National Natural Science Foundation of China (Grant No. 11175171). Special thanks are given to X. Wang from NUS for assistance in polishing up this paper.

[1] H. Fritze, H.L. Tuller, Appl. Phys. Lett. 78 (2001) 976.
[2] H. Fritze, H.L. Tuller, H. She, G. Borchardt, Sens. Actuators B 76 (2001) 103.
[3] R.C. Turner, P.A. Fuierer, R.E. Newnham, T.R. Shrout, Appl. Acoust. 41 (1994) 299.
[4] M.J. Davis, P. Vullo, I. Mitra, P. Blaum, K.A. Gudgel, N.J. Donnelly, C.A. Randall, J. Am. Ceram. Soc. 91 (2008) 2878.
[5] A. Halliyal, A.S. Bhalla, R.E. Newnham, L.E. Cross, J. Mater. Sci. 16 (1981) 1023.
[6] M.L. Zhao, L.H. Wang, C.L. Wang, J.L. Zhang, Z.G. Gai, C.M. Wang, J.C. Li, Appl. Phys. Lett. 95 (2009) 022904.
[7] M.L. Zhao, L.H. Wang, C.L. Wang, J.L. Zhang, Z.G. Gai, C.M. Wang, J.C. Li, Scripta Mater. 63 (2010) 207.
[8] R. Tararam, L.K. Bdikin, N. Panwar, J.A. Varela, P.R. Bueno, A.L. Kholkin, J. Appl. Phys. 110 (2011) 052019.
[9] J. Fousek, L.E. Cross, D.B. Litvin, Mater. Lett. 39 (1999) 287.
[10] L.E. Cross, J. Mater. Sci. 41 (2006) 53.
[11] W.Y. Zhu, J.Y. Fu, N. Li, L.E. Cross, Appl. Phys. Lett. 89 (2006) 192904.
[12] J.Y. Fu, W.Y. Zhu, N. Li, N.B. Smith, L.E. Cross, Appl. Phys. Lett. 91 (2007) 182910.
[13] J.F. Scott, M. Dawber, Appl. Phys. Lett. 76 (2000) 3801.
[14] M.W. Chu, I. Szafraniak, R. Scholz, C. Harnagea, D. Hesse, M. Alexe, U. Gosele, Nat. Mater. 3 (2004) 87.
[15] G. Catalan, B. Noheda, J. McAneney, L.J. Sinnamon, J.M. Gregg, Phys. Rev. B 72 (2005) 020102.
[16] D. Balzar, P.A. Ramakrishnan, A.M. Hermann, Phys. Rev. B 70 (2004) 092103.
[17] J.L. Maurice, F. Pailloux, A. Barthelemy, O. Durand, D. Imhoff, R. Lyonnet, A. Rocher, J.P. Contour, Philos. Mag. 83 (2003) 3201.
[18] R. Krause-Rehberg, H.S. Leipner, Positron Annihilation in Semiconductors, Springer Verlag, Berlin, 1998.
[19] P.G. Coleman, Positron Beams and Their Applications, World Scientific, Singapore, 2000.
[20] J. Cizek, O. Melikhova, M. Janecek, O. Srba, Z. Barnovska, I. Prochazka, S. Dobatkin, Scripta Mater. 65 (2011) 171.
[21] J. Cizek, O. Melikhova, I. Prochazka, J. Kuriplach, R. Kuzel, G. Brauer, W. Anwand, T.E. Konstantinova, I.A. Danilenko, Phys. Rev. B 81 (2010) 024116.
[22] J. Kansy, Nucl. Instrum. Methods Phys. Res. A 374 (1996) 235.
[23] P.J. Hautojarvi, Mater. Sci. Forum 175–178 (1995) 47.